An analytically based computer model for surface measurements in ultrasonic crack detection

Evgeny Glushkov, Natalia Glushkova, Alexander Ekhlakov, Elena Shapar
Kuban State University, Krasnodar, Russia
evg@math.kubsu.ru

Abstract

A low-cost computer model for ultrasonic detection of arbitrarily shaped and oriented planar cracks in an elastic half-space is presented. The model is based on the use of the integral equation technique and asymptotics derived from the oscillate integrals. The implementation of the method are illustrated by numerical examples.

1 Introduction

Traditionally the data processing of ultrasonic non-destructive testing (NDT) has relied upon ray methods of general diffraction theory similar to those used in geometrical optics [1, 2]. In view of the asymptotic nature of the ray approach, it is used in the high-frequency band, when the wavelength of the probing signal is much less than the characteristic dimension of the defect. On the other hand, if the dimensions of the defect are comparable with or less than the wavelength, reliable mathematical models become particularly important, since the reflection in this case gives a very blurred image, which requires special processing to size and shape the defect.

In this case a solution can be obtained by direct numerical methods like FEM, BEM or Finite Differences. However, these methods are time consuming and fail to provide insight into the mechanics of wave interaction processes.

The integral equation approach [3, 4] holds an intermediate position between the ray and direct numerical methods combining their advantages. On one hand, it gives a numerical solution like FEM, while being significantly less computationally intensive. On the other hand, asymptotic derivation of the integrals gives the same physically significant expressions as the ray-based approaches, while retaining in contrast the critical information about sources, structures and scatterers required for the reconstruction process.

Therefore, the integral equation method gives the chance to discover and explore fine wave phenomena that are usually overlooked with other approaches. It allowed us in particular to investigate the structure of time-averaged energy flows in layered and stepped waveguides with energy vortices and backward fluxes [5, 6], as well as to clear up their role in resonance extinguishing of surface waves [7].

In this paper we present a low-cost computer model for ultrasonic detection of arbitrarily shaped and oriented planar cracks in an elastic half-space. The model is based on the intensive use of the integral equation technique and asymptotics derived from the oscillate integrals. Typically, there are three problems of self-dependent interest: 1) calculation of an incident field $\mathbf{u}_0$, excited by a given source, 2) computation of the scattered field $\mathbf{u}_1$, diffracted by some obstacles (cracks, inclusions, etc.), and 3) accounting for the field $\mathbf{u}_2$, re-reflected from the sample surface, to be able to model a surface imprint of the scattered waves (Fig. 1).

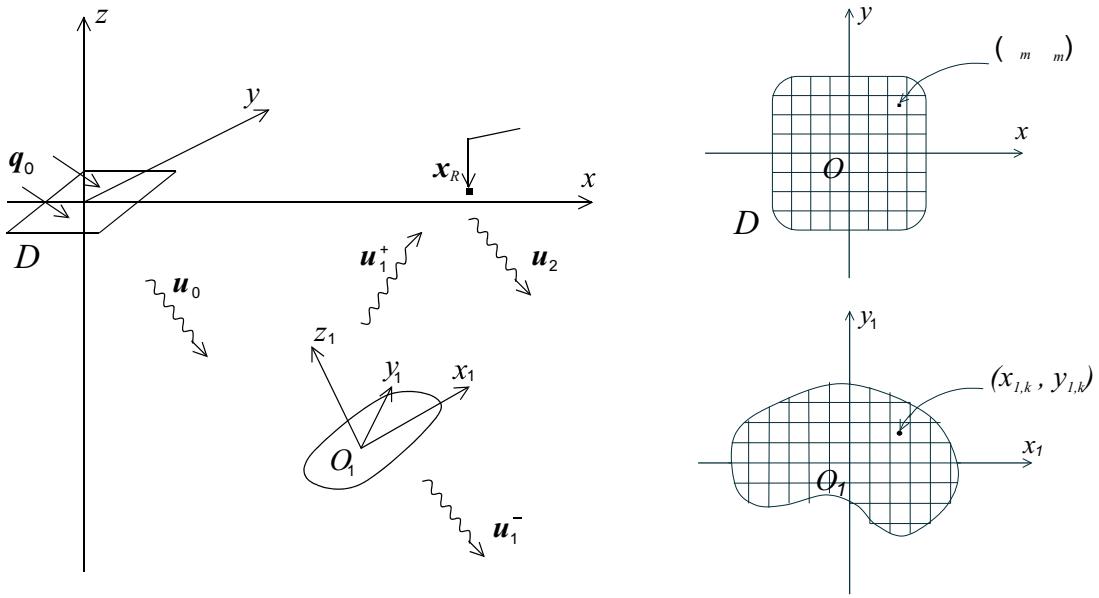

Figure 1: Geometry of the problem

Within the integral equation technique, $\mathbf{u}_0$ is derived explicitly in terms of a convolution of the half-space Green's matrix k with a given surface load $\mathbf{q}_0$ (see section 3 below), while $\mathbf{u}_1$ and $\mathbf{u}_2$ are to be obtained through the numerical solution of the boundary integral equations (BIEs) arisen from satisfaction boundary conditions on the defect's and sample's surfaces. There possible two situations: 1) a crack is deepened rather far from the surface, so that these fields can be calculated via successive solutions of practically independent diffraction (for $\mathbf{u}_1$) and reflection (for $\mathbf{u}_2$) problems; 2) with a near-surface or surface-breaking crack the mutual influence of the fields $\mathbf{u}_1$ and $\mathbf{u}_2$ is so strong that successive iterations are practically inapplicable and they have to be obtained, therefore, simultaneously from a more complicated BIE, which matrix-kernel accounts strictly for an infinite sequence of all re-reflections between the crack and half-space surfaces.

In the first case, the integral equations are well-known hypersingular BIEs with respect to an unknown crack opening displacement (c.o.d.) $\mathbf{v}$; their right-hand sides depend on the incident field $\mathbf{u}_0$. The field $\mathbf{u}_2$ can also appear in the right-hand sides within a successive specification of re-reflected fields. In this process the integral operator in the left-hand

side of the BIEs remains the same to be an operator with a matrix-kernel l_1 derived for a crack in an unbounded elastic space (section 4).

There has been developed a variety of approaches to their numerical solution (e.g. [9-13]) to be the key step of NDT models elaboration. To avoid the problem of kernel singularity we use a variational Galerkin scheme in the Fourier transform domain with the radial trial and test basis functions [13]. The far-field asymptotics of $\mathbf{u}_1$ (scattering diagrams) are derived from the integral representation of the diffracted field via the c.o.d. $\mathbf{v}$.

As for the reflected field, it seems natural to use the laws of ray reflection from a free surface [14] to obtain $\mathbf{u}_2$. However, more accurate asymptotics of $\mathbf{u}_2$ has also been derived directly from the integral representation, which connects $\mathbf{u}_2$ with the incident on the surface $z = 0$ field $\mathbf{u}_1$ explicitly (section 5). That explicit integral relation derived for an arbitrarily inclined crack allowed us, in addition, to arrive at the BIE with a modified kernel required in the second case of near-surface cracks (section 6). Its solution assures rigorous satisfaction of the stress-free boundary conditions on the both crack and half-space surfaces.

The model developed is illustrated by numerical examples of wave patterns and transient pulses acquired at the half-space surface (section 7).

2 Description of the Problem

Let us consider an elastic isotropic half-space containing an arbitrarily oriented and shaped planar crack. In a global Cartesian coordinate system (x, y, z) the half-space occupies the lower volume $-\infty \le x, y \le \infty,\ -\infty \le z \le 0$, while the crack is an infinitesimally thin material discontinuity with traction-free sides in a plane domain $(x_1, y_1) \in \Omega, z_1 = 0$. Here (x_1, y_1, z_1) is a local coordinate system connected with the crack (Fig. 1).

With obvious modifications the mathematical technique used below is applicable with any stratified medium which elastic constants are piecewise functions of z and does not depend on horizontal coordinates x, y (e.g. for interface crack detection [15]). However, for clarity sake we shall restrict our consideration to an isotropic homogeneous half-space.

The crack's location and orientation in the global system is fixed by the coordinates $\mathbf{x}_c$ of the centre of the local system in the global one and by a rotation matrix C setting a one to one connection between the coordinates of a point in the global $(\mathbf{x})$ and the local $(\mathbf{x}_1)$ systems:

$$\mathbf{x}_1 = C(\mathbf{x} - \mathbf{x}_c), \qquad \mathbf{x} = \mathbf{x}_c + C_1\mathbf{x}_1, \qquad C_1 = C^{-1} \tag{2.1}$$

The action of a probe (of an ultrasonic transducer) upon the medium is modeled by a given time-harmonic load $\mathbf{q}_0 e^{-i\omega t}$ applied to the traction-free surface $z = 0$ in a contact domain D:

$$\boldsymbol{\tau}(\mathbf{x})|_{z=0} = \begin{cases} \mathbf{q}_0(x, y), & (x, y) \in D \\ 0, & (x, y) \notin D \end{cases} \tag{2.2}$$

Here $\boldsymbol{\tau} = T_z\mathbf{u} = \{\tau_{xz}, \tau_{yz}, \sigma_z\}$ is a surface stress vector and D is a contact area between the source and the tested sample; $T_z = T_n$ with $\mathbf{n} = (0, 0, 1)$, where T_n is a stress operator

which yields a stress vector $\boldsymbol{\tau}$ relating to a field $\mathbf{u}$ at an area element fixed by a unit normal $\mathbf{n}$: $\boldsymbol{\tau} = T_n\mathbf{u} \equiv \lambda\mathbf{n}\mathrm{div}\,\mathbf{u} + 2\mu\partial\mathbf{u}/\partial n + \mu(\mathbf{n} \times \mathrm{curl}\,\mathbf{u})$; λ, μ are Lamé parameters of the elastic medium.

Depending on the type of the transducer, the contact area can be of different form (elliptic, rectangle or even disconnected: $D = \cup_m D_m$ for a system of sources). Function $\mathbf{q}_0$ sets the load distribution in D depending on the source characteristics (longitudinal or transverse, directional, inclined, etc). To model a realistic probe, $\mathbf{q}_0$ ought to be chosen in accordance with the law of traction distribution in the interface between the transducer and the tested material when it is caused by an incident plane wave coming from the electrically excited beveled edge of the transducer's piezo-crystal. This law is easily derived if the effect of finiteness of D is neglected [14, 16]. Otherwise, $\mathbf{q}_0$ is defined via solution of the Wiener-Hopf type integral equation, to which the contact problem is reduced [4]. Furthermore, we consider $\mathbf{q}_0$ as a known function.

Since any transient pulse $\mathbf{u}(\mathbf{x}, t)$ can be expressed as a linear superposition of the harmonic solutions $\mathbf{u}(\mathbf{x}, \omega)e^{-i\omega t}$:

$$\mathbf{u}(\mathbf{x}, t) = \frac{1}{\pi}\mathrm{Re}\int\limits_0^\infty \mathbf{u}(\mathbf{x}, \omega)e^{-i\omega t}d\omega, \tag{2.3}$$

we start from the harmonic steady-state problem with a circular frequency ω, omitting further the harmonic factor $e^{-i\omega t}$.

The main idea of the proposed approach is to compose the total field $\mathbf{u}$ of the source field $\mathbf{u}_0$, the scattered field $\mathbf{u}_1$ and the reflected field $\mathbf{u}_2$:

$$\mathbf{u} = \mathbf{u}_0 + \mathbf{u}_1 + \mathbf{u}_2 \tag{2.4}$$

using their explicit integral representations in terms of the half-space Green's matrix k, a given load $\mathbf{q}_0$, and an unknown c.o.d. $\mathbf{v}$. In such a partition $\mathbf{u}_0$ is the wave field obeying the boundary condition (2.2) at the half-space surface and the radiation condition at infinity. It is continuous inside the half-space while the diffracted field $\mathbf{u}_1$ is discontinuous at the crack with the jump (c.o.d.)

$$\mathbf{v} = (\mathbf{u}_1^+ - \mathbf{u}_1^-)|_{z_1=0}, \quad (x_1, y_1) \in \Omega \tag{2.5}$$

Here $\mathbf{u}_1^\pm$ are parts of $\mathbf{u}_1$ at the different sides of the crack plane $z_1 = 0$ written in the local coordinates $\mathbf{x}_1$ ($\mathbf{u}_1^+$ for $z_1 \geq 0$ and $\mathbf{u}_1^-$ for $z_1 \leq 0$).

This field $\mathbf{u}_1$ alone does not meet boundary conditions, hence the reflected field $\mathbf{u}_2$ is introduced to comply the stress-free condition at the surface $z = 0$ remaining after realization (2.2) by $\mathbf{u}_0$:

$$T_z(\mathbf{u}_1 + \mathbf{u}_2)|_{z=0} = 0 \tag{2.6}$$

Then, the stress-free condition at the crack sides must be satisfied by the superposition of all these three fields:

$$T_n(\mathbf{u}_0 + \mathbf{u}_1 + \mathbf{u}_2)|_{z_1=0} = 0 \tag{2.7}$$

Here T_n is the stress operator defined under (2.2) with $\mathbf{n}$ to be a unit normal to the crack plane.

In line with the physical matter of the process, the field $\mathbf{u}_c = \mathbf{u}_1 + \mathbf{u}_2$ caused by the presence of crack may be understood as an infinite succession of recurrent fields, diffracted by the crack and reflected from the surface:

$$\begin{aligned} \mathbf{u}_1 &= \mathbf{u}_1^{(1)} + \mathbf{u}_1^{(2)} + \mathbf{u}_1^{(3)} + \cdots \\ \mathbf{u}_2 &= \mathbf{u}_2^{(1)} + \mathbf{u}_2^{(2)} + \mathbf{u}_2^{(3)} + \cdots \end{aligned} \tag{2.8}$$

Here, $\mathbf{u}_1^{(1)}$ is the field scattered by the crack in the whole space due to the $\mathbf{u}_0$ incidence; $\mathbf{u}_2^{(1)}$ is the reflected field due to $\mathbf{u}_1^{(1)}$ incidence on the surface $z = 0$; $\mathbf{u}_1^{(2)}$ is due to $\mathbf{u}_2^{(1)}$ scattering by the crack, and so on.

With such a partition boundary conditions (2.6) and (2.7) also split up into a chain of equalities with respect to subfields $\mathbf{u}_1^{(i)}$ and $\mathbf{u}_2^{(i)}$, $i = 1, 2, \ldots$:

$$\begin{aligned} T_n(\mathbf{u}_0 + \mathbf{u}_1^{(1)})|_{z_1=0} &= 0 \qquad & T_z(\mathbf{u}_1^{(1)} + \mathbf{u}_2^{(1)})|_{z=0} &= 0 \\ T_n(\mathbf{u}_2^{(1)} + \mathbf{u}_1^{(2)})|_{z_1=0} &= 0 \qquad & T_z(\mathbf{u}_1^{(2)} + \mathbf{u}_2^{(2)})|_{z=0} &= 0 \\ \cdots & \qquad & \cdots & \\ T_n(\mathbf{u}_2^{(i-1)} + \mathbf{u}_1^{(i)})|_{z_1=0} &= 0 \qquad & T_z(\mathbf{u}_1^{(i)} + \mathbf{u}_2^{(i)})|_{z=0} &= 0 \\ \cdots & \qquad & \cdots & \end{aligned} \tag{2.9}$$

With a deepened crack and the Auld's electromechanical reciprocity argument technique [17], in many cases it is quite enough to take into account only the first scattered term $\mathbf{u}_1^{(1)}$ to be able to simulate adequately scan-images measured in practice with probes and/or receivers moving over the surface [16, 15]. A contribution of the next terms of expansions (2.8) into the Auld's argument $\delta\Gamma$ becomes tangible only with near-surface and surface-breaking cracks. In such a case the boundary element or boundary integral equation approach is applied to obtain the scattered and reflected fields by simultaneously satisfying boundary conditions (2.6), (2.7) at the sample surface and crack's sides without any recurrent chains of re-reflections [18, 19]. There is no need for any further terms in this case, because the mutual influence of the scattered and reflected fields $\mathbf{u}_1$ and $\mathbf{u}_2$ is taken into account strictly via BIEs.

A new need in the calculation of the summary field $\mathbf{u}_c = \mathbf{u}_1 + \mathbf{u}_2$ at the surface even with deepened cracks grew recently out of the laser measurement technique (e.g. see [20]). The laser acquirement of data from many surface points simultaneously is much faster than by transducers, but to simulate those data one has to compute the wave field $\mathbf{u}_c$ at the surface instead of using Auld's coefficient $\delta\Gamma$. With the laser measurements, a procedure of the crack form reconstruction can be based upon a fast parametrical analysis of the field $|\mathbf{u}_c|$ patterns on the surface.

3 The Probe Field

3.1 Integral Representation

Let $k(\mathbf{x})$ be a matrix which columns $\mathbf{k}_j(\mathbf{x})$ are displacement vectors associated with the surface point loads $\boldsymbol{\tau}|_{z=0} = \delta(\mathbf{x})\mathbf{e}_j$, $j = 1, 2, 3$ and the radiation condition at infinity. Here

δ is the Dirac function and $\mathbf{e}_j$ are the unit coordinate vectors for the axes Ox, Oy, Oz respectively. This matrix k is referred to as the *half-space Green's matrix*. With the matrix k any displacement resulted from a surface load, including the probe field $\mathbf{u}_0$, can be expressed in terms of the convolution integral

$$\mathbf{u}_0(\mathbf{x}) = \iint\limits_D k(\mathbf{x} - \boldsymbol{\xi})\mathbf{q}_0(\xi, \eta)d\xi d\eta, \quad \boldsymbol{\xi} = \{\xi, \eta, 0\} \tag{3.1}$$

Obviously, $\mathbf{u}_0$ complies with the boundary condition (2.2).

The Fourier transform technique allows one to derive half-space Green's matrix in terms of path Fourier integrals:

$$k(\mathbf{x}) = \mathcal{F}^{-1}[K] \equiv \frac{1}{(2\pi)^2} \iint\limits_{\Gamma_1\Gamma_2} K(\alpha_1, \alpha_2, \alpha, z)e^{-i(\alpha_1 x + \alpha_2 y)}d\alpha_1 d\alpha_2 \tag{3.2}$$

where $\alpha = \sqrt{\alpha_1^2 + \alpha_2^2}$, matrix $K = \mathcal{F}[k]$ is the Fourier transform of $k(\mathbf{x})$ over x, y (Fourier symbol); by $\mathcal{F}$ and $\mathcal{F}^{-1}$ we denote direct and inverse transforms.

The contours Γ_1 and Γ_2 go in the complex planes α_1, α_2 along the real axes $\operatorname{Im}\alpha_n = 0$, $n = 1, 2$, deviating from them for bypassing real poles and branch points of the matrix K elements. The directions of the deviation are governed by the principle of limiting absorption [4].

It is worthy to note that representation (3.1) – (3.2) remains valid with any piecewise continuous dependence of elastic properties on z (e.g. for a multi-layered half-space or a laminated plate). For an isotropic homogeneous half-space the symbol K is of the following structure (in the conventional notation introduced by Vorovich and Babeshko [4]): $K = K^-$ (K^+ is for the upper half-space $z > 0$) and

$$K^{\pm}(\alpha_1, \alpha_2, \alpha, z) = \sum_{n=1}^{2} K_n^{\pm}(\alpha_1, \alpha_2, \alpha)e^{-\sigma_n|z|} \tag{3.3}$$

with

$$K_n^{\pm} = \frac{1}{\Delta}\begin{pmatrix} \pm i(\alpha_1^2 M_n + \alpha_2^2 N_n) & \pm i\alpha_1\alpha_2(M_n - N_n) & -i\alpha_1 P_n \\ \pm i\alpha_1\alpha_2(M_n - N_n) & \pm i(\alpha_1^2 N_n + \alpha_2^2 M_n) & -i\alpha_2 P_n \\ \alpha_1 S_n & \alpha_2 S_n & \mp R_n \end{pmatrix}$$

$$\begin{array}{ll} M_1 = i\sigma_2 & M_2 = -i\sigma_2\gamma^2/\alpha^2 \\ P_1 = -\gamma^2 & P_2 = \sigma_1\sigma_2 \\ S_1 = i\sigma_1\sigma_2 & S_2 = -i\gamma^2 \\ R_1 = -\sigma_1\gamma^2 & R_2 = \sigma_1\alpha^2 \\ N_1 = 0 & N_2 = i\Delta/(\mu\alpha^2\sigma_2) \end{array} \tag{3.4}$$

$$\Delta(\alpha) = 2\mu(-\gamma^4 + \alpha^2\sigma_1\sigma_2), \quad \gamma^2 = \alpha^2 - 0.5\kappa_2^2$$

$$\sigma_n(\alpha) = \sqrt{\alpha^2 - \kappa_n^2}, \quad \kappa_n = \omega/v_n, \ n = 1, 2;$$

v_1, v_2 are velocities of the longitudinal and transverse (P and S) body waves, κ_1, κ_2 are corresponding wave numbers. The branches of the radicals are fixed in the complex plane

α by the cuts $\alpha(t) = \pm\sqrt{\kappa_n^2 - t^2}, 0 \le t \le \infty$ and conditions $\sigma_n(\alpha) \to \infty$ as $\alpha^2 \to \infty$, so that no growing exponents occur in any K component as $|\alpha| \to \infty$ or $z \to -\infty$.

Functions M_n, N_n, P_n, R_n, S_n and Δ in (3.3) depend only on α, therefore, the change of variables

$$\left\{ \begin{array}{l} \alpha_1 = \alpha\cos\gamma \\ \alpha_2 = \alpha\sin\gamma \end{array} \right. \quad \left\{ \begin{array}{ll} x = r\cos\varphi & \alpha = \sqrt{\alpha_1^2 + \alpha_2^2} \\ y = r\sin\varphi & r = \sqrt{x^2 + y^2} \end{array} \right. \tag{3.5}$$

together with the Bessel functions representation [21]:

$$2\pi i^n J_n(\alpha r) = \int_0^{2\pi} e^{i\alpha r\cos\gamma - in\gamma} d\gamma \tag{3.6}$$

brings (3.2) to a one-dimensional path integral form:

$$k(\mathbf{x}) = \frac{1}{2\pi}\int_\Gamma K(i\partial/\partial x, i\partial/\partial y, \alpha, z) J_0(\alpha r)\alpha d\alpha. \tag{3.7}$$

The contour Γ is resulted from Γ_1, Γ_2 in accordance with the change (3.5). It goes in the complex plane α along the real positive axis $\mathrm{Im}\,\alpha = 0$, $\mathrm{Re}\,\alpha > 0$ also bypassing real positive poles ζ_m and branch points κ_n of the integrands. With the homogeneous medium considered, there is the only Rayleigh real pole $\zeta:\ \Delta(\zeta) = 0$.

The multipliers α_1, α_2 are substituted in K by the space derivatives by virtue of the one-to-one correspondence

$$\alpha_1^{p_1}\alpha_2^{p_2} \leftrightarrow \left(i\frac{\partial}{\partial x}\right)^{p_1}\left(i\frac{\partial}{\partial y}\right)^{p_2},\ p_1, p_2 = 0, 1, 2$$

Their acting on the Bessel function yields the Bessel functions again [21]:

$\frac{\partial}{\partial x}J_0(\alpha r) = -\alpha\cos\varphi J_1(\alpha r)$,

$\frac{\partial^2}{\partial x^2}J_0(\alpha r) = \alpha^2[(\sin^2\varphi - \cos^2\varphi)\frac{J_1(\alpha r)}{\alpha r} + \cos\varphi J_0(\alpha r)]$, etc.

so that no derivatives remain in the final integral representation. It should be noted that such representation can also be derived directly from (3.2) without derivatives in (3.7), just by substituting $\sin^p\gamma, \cos^p\gamma, p = 1, 2$ into (3.3) accordingly (3.5) in terms of exponents $e^{\pm in\gamma}$, which are accounted then in (3.6).

3.2 Far-field asymptotics

The derived integral representation (3.1) – (3.7) is quite applicable for a direct numerical obtaining of the incident field $\mathbf{u}_0(\mathbf{x})$ in a near-field zone, where the distance from the source $R = |\mathbf{x}|$ is commensurable with a wavelength l. However, the near-field is of little interest for the crack detection, whereas computing expenses increase dramatically as $R/l >> 1$, up to practical inapplicability at a certain distance. Therefore, the integral representation is used mostly as the starting point for the derivation of far-field asymptotics.

The contribution of the pole ζ, derived using the residual technique, yields the surface Rayleigh wave:

$$\mathbf{u}_R(\mathbf{x}) = \mathbf{b}(\varphi, z)e^{i\zeta r}/\sqrt{r} + O(r^{-3/2}) \quad \text{as} \quad r \to \infty,\ z = \text{const} \tag{3.8}$$

where $\mathbf{b} = \sqrt{i\zeta/(2\pi)}B(\varphi, z)\mathbf{Q}_R(\varphi)$

$$B = \operatorname{res} K|_{\alpha=\zeta} = \hat{K}(-\zeta\cos\varphi, -\zeta\sin\varphi, \zeta, z)/\Delta'(\zeta)$$

$$\hat{K}:\ K = \hat{K}/\Delta, \quad \mathbf{Q}_R = \mathbf{Q}_0(-\zeta\cos\varphi, -\zeta\sin\varphi)$$

$$\mathbf{Q}_0(\alpha_1, \alpha_2) = \mathcal{F}[\mathbf{q_0}] = \iint\limits_D \mathbf{q}_0(x, y)e^{i(\alpha_1 x + \alpha_2 y)}dxdy.$$

Since $\mathbf{u}_R(\mathbf{x})$ is localized near the surface ($B(\varphi, z)$ decreases exponentially as $z \to -\infty$), the contribution of $\mathbf{u}_R$ in the total asymptotic expansion only matters for distant detection of near-surface cracks. The deepened defects are illuminated by the body waves, which asymptotics are derived from (3.1), (3.2) by the steepest descent method [5].

At first, the stationary points

$$\alpha_{1,n} = -\kappa_n\cos\varphi\sin\psi,\ \ \alpha_{2,n} = -\kappa_n\sin\varphi\sin\psi \tag{3.9}$$

of the oscillating exponential components $\exp(i(\sqrt{\kappa_n^2 - \alpha^2} - \alpha_1 x - \alpha_2 y))$ contributes in the asymptotics of the initial double integral (3.2) as follows:

$$k(\mathbf{x} - \boldsymbol{\xi}) = \sum_{n=1}^{2} k_n(\varphi, \psi)e^{i\kappa_n R}/R + O(R^{-2}) \quad \text{as } R \to \infty, \tag{3.10}$$

$$k_n = -i\kappa_n|\cos\psi|K_n(\alpha_{1,n}, \alpha_{2,n}, \alpha_n)/(2\pi)$$

$R = \sqrt{(x-\xi)^2 + (y-\eta)^2 + z^2}$, φ, ψ are the radius and angles of a spherical coordinate system centered at a current point $(\xi, \eta, 0)$:

$$\begin{cases} x - \xi = R\cos\varphi\sin\psi & 0 \le \varphi \le 2\pi \\ y - \eta = R\sin\varphi\sin\psi & \\ z = R\cos\psi & \pi/2 < \psi \le \pi \end{cases}$$

Two terms of the sum (3.10) describe spherical P and S waves for $n = 1$ and $n = 2$ respectively.

Then, replacing the convolution integral (3.1) with an approximate cubature formula with nodes $(\xi_m, \eta_m) \in D$, $m = 1, 2, ..., M$, we arrive at the body wave asymptotics of $\mathbf{u}_0$ in the half-space:

$$\mathbf{u}_0(\mathbf{x}) \sim \sum_{n=1}^{2}\sum_{m=1}^{M} k_n(\varphi_m, \psi_m)\mathbf{q}_0(\xi_m, \eta_m)s_m e^{i\kappa_n R_m}/R_m \quad \text{as } R_m \to \infty,\ \psi > \pi/2 \tag{3.11}$$

in which φ_m, ψ_m, R_m are spherical coordinates of a point $\mathbf{x}$ in the systems centered at points $(\xi_m, \eta_m, 0)$; s_m are cubature weight coefficients.

4 The Scattered Field

With the set forth approach the scattered field $\mathbf{u}_1$ is represented in the same explicit integral form like $\mathbf{u}_0$, but via the unknown crack opening displacement $\mathbf{v}$, which is determined from the integral equations arising when the boundary conditions at the crack sides are satisfied. Let $\mathbf{q}_1 = T_n\mathbf{u}_1|_{z_1=0}$ be a traction vector at the crack plane $z_1 = 0$, associated with the field $\mathbf{u}_1$ (in the local coordinates $\mathbf{x}_1$). This unknown field can be expressed via $\mathbf{q}_1$ in the same manner as $\mathbf{u}_0$ through $\mathbf{q}_0$, i.e. using Green's matrices k^+, k^- for the upper and lower half-spaces $z_1 \geq 0$ and $z_1 \leq 0$. In the Fourier domain it takes the form

$$\mathbf{U}_1^{\pm}(\alpha_1, \alpha_2, z_1) = K^{\pm}(\alpha_1, \alpha_2, z_1)\mathbf{Q}_1(\alpha_1, \alpha_2) \tag{4.1}$$

while (2.5) is converted into

$$\mathbf{V}(\alpha_1, \alpha_2) = [K^+(\alpha_1, \alpha_2, 0) - K^-(\alpha_1, \alpha_2, 0)]\mathbf{Q}_1(\alpha_1, \alpha_2) \tag{4.2}$$

$$\mathbf{V} = \mathcal{F}[\mathbf{v}], \quad \mathbf{Q}_1 = \mathcal{F}[\mathbf{q}_1]$$

Equation (4.2) allows one to express $\mathbf{Q}_1$ through $\mathbf{V}$:

$$\mathbf{Q}_1 = L_1\mathbf{V}, \quad L_1(\alpha_1, \alpha_2) = (K^+ - K^-)^{-1}|_{z_1=0}, \tag{4.3}$$

hence, $\mathbf{q}_1 = \mathcal{F}^{-1}[L_1\mathbf{V}]$.

The integral equation with respect to unknown $\mathbf{v}$ follows then from the traction-free boundary conditions (2.6) and (2.7). First, let us consider a deepened crack, when re-reflections from far surfaces are neglected, that is when one can take $\mathbf{u}_1 = \mathbf{u}_1^{(1)}$ (see (2.8)) without loss of accuracy. Only the first of the conditions (2.9) is required for determining $\mathbf{v} = \mathbf{v}^{(1)}$ in this case:

$$(\mathbf{q}_1 + \boldsymbol{\tau}_0)|_{z_1=0} = 0, \quad (x_1, y_1) \in \Omega \tag{4.4}$$

Here $\boldsymbol{\tau}_0 = CT_n\mathbf{u}_0$ is a known traction vector at the crack plane related to the incident field $\mathbf{u}_0$, C is the rotating matrix from (2.1) giving coordinates $\boldsymbol{\tau}_0$ in the local system. Eqs. (4.3) and (4.4) lead to the Wiener-Hopf integral equation

$$\mathcal{L}_1\mathbf{v} \equiv \iint\limits_{\Omega} l_1(\mathbf{x_1} - \boldsymbol{\xi}_1)\mathbf{v}(\xi, \eta)d\xi d\eta = \mathbf{g}(x_1, y_1), \quad (x_1, y_1) \in \Omega \tag{4.5}$$

where $l_1(\mathbf{x}_1) = \mathcal{F}^{-1}[L_1]$, $\mathbf{g} = -\boldsymbol{\tau}_0|_{z_1=0}$.

To solve eq. (4.5) with an arbitrary domain Ω, we use a variational Galerkin scheme with axially symmetric (radial) δ-like trial and test functions f_k set at the nodes $(x_{1,k}, y_{1.k})$ covering Ω with a spacing h [13]:

$$\mathbf{v} \approx \mathbf{v}_N(x_1, y_1) = \sum_{k=1}^{N} \mathbf{v}_k f_k(x_1, y_1) \tag{4.6}$$

$\mathbf{v}_k$ are expansion coefficients, $f_k = f((x_1 - x_{1,k})/h, (y_1 - y_{1,k})/h)$, where $f(x, y) = f(r), r = \sqrt{x^2 + y^2}$ is a radial shape function of the basis, N is a number of the nodes. Consequently,

$$\mathbf{V}(\alpha_1,\alpha_2)\approx\mathbf{V}_N(\alpha_1,\alpha_2)=h^2\sum_{k=1}^{N}\mathbf{v}_k e^{i(x_{1,k}\alpha_1+y_{1,k}\alpha_2)}F(\alpha), \tag{4.7}$$

$F(\alpha)=\mathcal{F}[f]$.

Unknown vectors $\mathbf{v}_k$ are obtained from the linear algebraic system to which equation (4.5) is reduced in line with the Galerkin scheme. The axial symmetry of f allowed us to gain the most benefit in reducing numerical costs spent on $\mathbf{v}$ obtaining. With Green's matrices $k^{\pm}$ and expansion (4.6), integral representation of the scattered field $\mathbf{u}_1$ in the crack coordinate system takes the form

$$\mathbf{u}_1^{\pm}(\mathbf{x}_1)\approx\frac{1}{(2\pi)^2}\sum_{k=1}^{N}\iint\limits_{\Gamma_1\Gamma_2}\mathbf{U}_{1,k}^{\pm}(\alpha_1,\alpha_2,z_1)e^{-i(\alpha_1(x_1-x_{1,k})+\alpha_2(y_1-y_{1,k}))}d\alpha_1 d\alpha_2 \tag{4.8}$$

where $\mathbf{U}_{1,k}^{\pm}=K^{\pm}(\alpha_1,\alpha_2,\alpha,z)L_1(\alpha_1,\alpha_2)F(\alpha h)\mathbf{v}_k h^2$.

Far-field asymptotics follows from eq. (4.8) in the same way that asymptotics (3.11) follows from eq. (3.1):

$$\mathbf{u}_1^{\pm}(\mathbf{x}_1)\sim\sum_{n=1}^{2}\sum_{k=1}^{N}\mathbf{a}_{nk}^{\pm}(\varphi_k,\psi_k)e^{i\kappa_n R_k}/R_k,\quad R_k=|\mathbf{x}_1-\mathbf{x}_{1,k}|\to\infty \tag{4.9}$$

$$\mathbf{a}_{nk}^{\pm}=-i|\cos\psi_k|\kappa_n h^2 K_{nk}^{\pm}L_{nk}F_k\mathbf{v}_k/(2\pi),$$

$K_{nk}^{\pm},L_{nk},F_{nk}$ are values of matrices and functions K_n,L_1,F at the stationary points $\alpha_{1,nk},\alpha_{2,nk}$, $\alpha_{nk}=\sqrt{\alpha_{1,nk}^2+\alpha_{2,nk}^2}$, which are of form (3.9) again but with φ_k,ψ_k to be the angles of the local spherical coordinate systems centered in the nodes $(x_{1,k},y_{1,k},0)$:

$$\begin{cases} x_1-x_{1,k}=R_k\cos\varphi_k\sin\psi_k & 0\le\varphi_k\le 2\pi \\ y_1-y_{1,k}=R_k\sin\varphi_k\sin\psi_k & \\ z_1=R_k\cos\psi_k & 0<\psi_k\le\pi \end{cases}$$

Asymptotics (4.9) gives a fairy simple and fast approximation of the scattered field by the superposition of spherical P and S waves radiated by elementary sources located at the nodes $\mathbf{x}_{1,k}$ with amplitudes controlled by vectors $\mathbf{v}_k$. It is significant that representations (4.8), (4.9) are also true if $\mathbf{v}$ is obtained from a general BIE taking into account the influence of the reflected field $\mathbf{u}_2$ (e.g. from eq. (6.2) below).

We should add that the electromechanical reciprocity argument of Auld $\delta\Gamma$, which gives the same information that is measured in pulse-echo scanning practice [17, 16], can also be easily expressed through $\mathbf{v}$:

$$\delta\Gamma=-\frac{i\omega}{P}\iint\limits_{\Omega}\mathbf{v}\cdot\mathbf{g}\,d\Omega\approx-\frac{i\omega}{P}h^2\sum_{k=1}^{N}\mathbf{v}_k\cdot\mathbf{g}_k \tag{4.10}$$

$$\mathbf{g}_k=\mathbf{g}(x_{1,k},y_{1,k}),\quad \mathbf{v}\cdot\mathbf{g}=\sum_{i=1}^{3}v^{(i)}g^{(i)}$$

5 Reflection from the Surface

In regard to signals recorded at the half-space surface $z = 0$ we, in addition to the scattered field $\mathbf{u}_1$, have to take into account the field $\mathbf{u}_2$ reflected from this surface. Along with the possibility of obtaining $\mathbf{u}_2$ at the points of measurements using the well-known ray formulae for quasi-plane P and S waves reflection from a free surface [14], it is possible to express $\mathbf{u}_2$ through an auxiliary stress vector $\mathbf{q}_2 = -\boldsymbol{\tau}_1|_{z=0} = -T_z C_1 \mathbf{u}_1|_{z=0}$ induced at the surface by the incident field $\mathbf{u}_1$. In Fourier symbols it takes the same form

$$\mathbf{U}_2(\alpha_1, \alpha_2, z) = K(\alpha_1, \alpha_2, z)\mathbf{Q}_2(\alpha_1, \alpha_2) \tag{5.1}$$

with the same matrix $K = K^-$ like the representations of $\mathbf{u}_0$ and $\mathbf{u}_1$ above.

Hence, for a deepened crack we can derive the asymptotics required from the inverse Fourier transform $\mathbf{u}_2(\mathbf{x}) = \mathcal{F}^{-1}[\mathbf{U}_2]$ similarly to asymptotics (3.8),(3.11) for $\mathbf{u}_0$, i.e. as a contribution of integrand's poles and stationary points of oscillating exponents. The main problem here is to derive $\mathbf{Q}_2$ explicitly in the global coordinates starting from the expression for $\mathbf{u}_1$ in the local ones.

For a horizontal crack this problem is solved easily. The axes of the global and local coordinate systems can be taken collinearly, so that the derivatives, and consequently the stress operator T_z, remain the same in the both systems. For an inclined crack the mismatch of planes x_1y_1 and x, y, over which the Fourier transform is applied to $\mathbf{u}_1$ and to $\boldsymbol{\tau}_1$, implies cumbersome analytical calculations. To avoid these difficulties, we propose the next trick.

Let us, firstly, express $\mathbf{u}_1$ through the 3D Fourier integral:

$$\mathbf{u}_1(\mathbf{x}_1) = \frac{1}{(2\pi)^3} \int\limits_{\Gamma_1}\int\limits_{\Gamma_2}\int\limits_{\Gamma_3} \hat{\mathbf{U}}_1(\boldsymbol{\alpha}) e^{-i(\boldsymbol{\alpha}\cdot\mathbf{x}_1)} d\boldsymbol{\alpha} \tag{5.2}$$

in which

$$\hat{\mathbf{U}}_1(\boldsymbol{\alpha}) = \mathcal{F}_{z_1}[\mathbf{U}_1] \equiv \int\limits_{-\infty}^{\infty} \mathbf{U}_1(\alpha_1, \alpha_2, z_1) e^{i\alpha_3 z_1} dz_1$$

is a 3D Fourier symbol depending on the vector of Fourier parameters $\boldsymbol{\alpha} = (\alpha_1, \alpha_2, \alpha_3)$; $(\boldsymbol{\alpha}\cdot\mathbf{x}_1) = \alpha_1 x_1 + \alpha_2 y_1 + \alpha_3 z_1$. Starting from eq. (4.1) we arrive at

$$\hat{\mathbf{U}}_1(\boldsymbol{\alpha}) = \hat{K}(\boldsymbol{\alpha})\mathbf{Q}_1(\alpha_1, \alpha_2) \tag{5.3}$$

The explicit form of $\hat{K}(\boldsymbol{\alpha}) = \mathcal{F}_{z_1}[K^{\pm}(\alpha_1, \alpha_2, z_1)]$ is easily derived in so far as the transform $\mathcal{F}_{z_1}$ acts upon no more than two different simple functions of z_1 entering in $K^{\pm}(\alpha_1, \alpha_2, z_1)$ of form (3.3):

$$\mathcal{F}_{z_1}[e^{-\sigma_n|z_1|}] = 2\sigma_n/\delta_n(\boldsymbol{\alpha}) \quad \text{and} \quad \mathcal{F}_{z_1}[\mathrm{sign} z_1\, e^{-\sigma_n|z_1|}] = 2i\alpha_3/\delta_n(\boldsymbol{\alpha})$$

where $\delta_n(\boldsymbol{\alpha}) = \alpha_3^2 + \sigma_n^2 = |\boldsymbol{\alpha}|^2 - \kappa_n^2, n = 1, 2$. It results in the expression

$$\hat{K}(\boldsymbol{\alpha}) = \sum_{n=1}^{2} \hat{K}_n(\boldsymbol{\alpha})/\delta_n(\boldsymbol{\alpha}) \tag{5.4}$$

with

$$\hat{K}_n(\boldsymbol{\alpha}) = \frac{2}{\Delta(\alpha_1,\alpha_2)} \begin{pmatrix} -\alpha_3(\alpha_1^2 M_n + \alpha_2^2 N_n) & -\alpha_1\alpha_2\alpha_3(M_n - N_n) & -i\alpha_1\sigma_n P_n \\ -\alpha_1\alpha_2\alpha_3(M_n - N_n) & -\alpha_3(\alpha_1^2 N_n + \alpha_2^2 M_n) & -i\alpha_2\sigma_n P_n \\ \alpha_1\sigma_n S_n & \alpha_2\sigma_n S_n & -i\alpha_3 R_n \end{pmatrix}, \; n = 1, 2$$

Then, we can pass in eq. (5.2) into the global coordinates by the rotation $\mathbf{x}_1 = C(\mathbf{x} - \mathbf{x}_c)$ with the same rotation in the Fourier variables: $\boldsymbol{\alpha} = C\boldsymbol{\beta}$, $\boldsymbol{\beta} = (\beta_1, \beta_2, \beta_3)$. With those substitutions the power exponent keeps its form:

$$(\boldsymbol{\alpha}, \mathbf{x}_1) = (C\boldsymbol{\beta}, C(\mathbf{x} - \mathbf{x}_c)) = (\boldsymbol{\beta}, \mathbf{x}) - (\boldsymbol{\beta}, \mathbf{x}_c)$$

and vectors of Fourier parameters are also invariable in length: $|\boldsymbol{\alpha}| = |\boldsymbol{\beta}|$, $|\boldsymbol{\beta}|^2 = \beta_1^2 + \beta_2^2 + \beta_3^2$. In particular,

$$\delta_n(\boldsymbol{\alpha}) = \delta_n(\boldsymbol{\beta}) = |\boldsymbol{\beta}| - \kappa_n^2 = \beta_3^2 + \hat{\sigma}_n^2(\beta)$$

here $\hat{\sigma}_n(\beta) = \sqrt{\beta^2 - \kappa_n^2}$, $\beta^2 = \beta_1^2 + \beta_2^2$, $n = 1, 2$.

In the $\boldsymbol{\beta}$ domain application of the stress operator T_z is equal to multiplication by its Fourier symbol

$$T(\boldsymbol{\beta}) = -i\mu \begin{pmatrix} \beta_3 & 0 & \beta_1 \\ 0 & \beta_3 & \beta_2 \\ \delta\beta_1 & \delta\beta_2 & (\delta+2)\beta_3 \end{pmatrix}, \qquad \delta = \lambda/\mu$$

that is

$$\boldsymbol{\tau}_1(\mathbf{x}) = \frac{1}{(2\pi)^3} \iiint\limits_{\Gamma_1\Gamma_2\Gamma_3} T(\boldsymbol{\beta}) C_1 \hat{U}_1(C\boldsymbol{\beta}) e^{-i(\boldsymbol{\beta}, (\mathbf{x}-\mathbf{x}_c)} d\boldsymbol{\beta}$$

The explicit form of $\mathbf{Q}_2 = \mathcal{F}_{xy}[-\boldsymbol{\tau}_1(x, y, 0)]$ is easily derived then in terms of one-fold path integrals over Γ_3, which taking into account (5.3), (5.4) and (4.3) can be written in the following form

$$\mathbf{Q}_2(\beta_1, \beta_2) = -\frac{1}{2\pi} \int\limits_{\Gamma_3} T(\boldsymbol{\beta}) C_1 \sum_{n=1}^{2} \hat{K}_n(C\boldsymbol{\beta}) / \delta_n(\boldsymbol{\beta}) L_1(C\boldsymbol{\beta}) \mathbf{V}(C\boldsymbol{\beta}) e^{i(\boldsymbol{\beta}, \mathbf{x}_c)} d\beta_3$$

With the residual technique these integrals over β_3 can be calculated as a contribution of the poles $\beta_3 = -i\hat{\sigma}_n(\beta)$, which are the only roots of the denominators $\delta_n(\boldsymbol{\beta})$. As the result we arrive at the explicit analytical expression

$$\mathbf{Q}_2(\beta_1, \beta_2) = \sum_{n=1}^{2} \hat{M}_n(\beta_1, \beta_2) \hat{\mathbf{V}}_n(\beta_1, \beta_2) e^{i(\beta_1 x_c + \beta_2 y_c)} e^{\hat{\sigma}_n z_c} \tag{5.5}$$

where $\hat{M}_n(\beta_1, \beta_2) = -T(\boldsymbol{\beta}) C_1 \hat{K}_n(C\boldsymbol{\beta}) L_1(C\boldsymbol{\beta}) / (2\hat{\sigma}_n)|_{\beta_3 = -i\hat{\sigma}_n}$ and $\hat{\mathbf{V}}_n(\beta_1, \beta_2) = \mathbf{V}(C\boldsymbol{\beta}))|_{\beta_3 = -i\hat{\sigma}_n}$.

It is important to keep in mind that $\mathbf{Q}_2$ in the form (5.5) is derived for any crack, therefore, it is valid not only for deepened cracks but for sub-surface and surface-breaking ones too.

Let $\mathbf{x}_R = (x_R, y_R, 0)$ be a point on the surface $z = 0$ in which the reflected signal is recorded. With regard to eqs. (5.1), (5.5) and (4.7) the inverse integrals for $\mathbf{u}_2(\mathbf{x}_R)$ are brought to the form

$$\mathbf{u}_2(\mathbf{x}_R) \approx \frac{h^2}{(2\pi)^2} \sum_{n=1}^{2} \sum_{k=1}^{N} \iint\limits_{\Gamma_1\Gamma_2} K(\beta_1, \beta_2, \beta, 0) \hat{M}_n(\boldsymbol{\beta}) \hat{F}(\boldsymbol{\beta}) e^{\hat{\sigma}_n z_k} \mathbf{v}_k e^{-i(\beta_1(x_R - x_k) + \beta_2(y_R - y_k))} d\beta_1 d\beta_2 \tag{5.6}$$

where $\mathbf{x}_k = \mathbf{x}_c + C_1 \mathbf{x}_{1,k}$ are nodes $\mathbf{x}_{1,k} \in \Omega$ in the global system.

Then, the body-waves asymptotics of $\mathbf{u}_2(\mathbf{x}_R)$ as $R_k = \sqrt{(x_R - x_k)^2 + (y_R - y_k)^2 + z_k^2} \to \infty$ is derived from (5.6) by the same way as (3.11) for $\mathbf{u}_0$. It takes the form:

$$\mathbf{u}_2(\mathbf{x}_R) \sim \sum_{n=1}^{2} \sum_{k=1}^{N} \mathbf{b}_{nk}(\varphi_k, \psi_k) e^{i\kappa_n R_k} / R_k + O(R_k^{-2}), \quad R_k \to \infty \tag{5.7}$$

Here (φ_k, ψ_k, R_k) are spherical coordinates of the vectors $\mathbf{x}_R - \mathbf{x}_k$;

$$\mathbf{b}_{nk} = -i\kappa_n |\cos\psi_k| K(\beta_{1,nk}, \beta_{2,nk}, 0) \hat{M}_n(\boldsymbol{\beta}_{nk}) \hat{F}(\boldsymbol{\beta}_{nk}) \mathbf{v}_k h^2/(2\pi)/(-2\hat{\sigma}_{nk})$$

$$\begin{cases} \beta_{l,nk} = -\kappa_n \cos\varphi_k \sin\psi_k, \quad \beta_{nk} = \sqrt{\beta_{1,nk}^2 + \beta_{2,nk}^2} \\ \beta_{2,nk} = -\kappa_n \sin\varphi_k \sin\psi_k \end{cases}$$

Thus, quite similarly to $\mathbf{u}_1$, at a far distance from the crack the field $\mathbf{u}_2(\mathbf{x}_R)$ is added up from spherical body waves radiated by elementary sources located in the crack domain Ω at the nodes $\mathbf{x}_k$ and controlled by the vector coefficients $\mathbf{v}_k$ but with the angle vector-functions $\mathbf{b}_{nk}$ accounting in addition for the reflection from the surface $z = 0$ and crack's incline.

It is worthy to note that the contribution of the Rayleigh pole ζ into $\mathbf{u}_2(\mathbf{x}_R)$ vanishes exponentially as $z_k \to -\infty$ due to the factors $e^{\hat{\sigma}_n z_k}$ in the integrand (5.6).

6 Near-surface cracks

With near-surface cracks integral equation (4.5) fails to satisfy the total boundary condition on the crack sides due to a tangible influence of the reflected field. In this case the integral equation has to be derived from the condition (2.7)

$$(\mathbf{q}_1 + CT_n \mathbf{u}_2 + \boldsymbol{\tau}_0)|_{z_1=0} = 0, \quad (x_1, y_1) \in \Omega \tag{6.1}$$

instead of eq. (4.4). Since, in line with (5.1) and (5.5), $T_n \mathbf{u}_2$ is also expressed via $\mathbf{v}$, the resulting integral equation becomes of the form

$$\mathcal{L}_1 \mathbf{v} + \mathcal{L}_2 \mathbf{v} \equiv \iint\limits_{\Omega} [l_1(\mathbf{x}_1 - \boldsymbol{\xi}_1) + l_2(\mathbf{x}_1, \boldsymbol{\xi}_1)] \mathbf{v}(\boldsymbol{\xi}_1) d\boldsymbol{\xi}_1 = \mathbf{g}(x_1, y_1), \quad (x_1, y_1) \in \Omega \tag{6.2}$$

in which kernel l_1 remains the same like in eq. (4.5) while the Fourier symbol of l_2 is expressed via the part of $\mathbf{Q}_2$ (except $\mathbf{v}$) multiplied by CT_nK from the left. This

equation takes explicitly into account all successive recurrent reflections from the crack and boundaries which affect on the crack open displacement $\mathbf{v}$.

If the crack does not touch the surface, the Fourier symbol of l_2 decreases exponentially as $\alpha \to \infty$ due to the $\mathbf{Q}_2$ structure. Therefore, in this case the kernel l_2 is a smooth matrix-function of $\mathbf{x}$ and $\boldsymbol{\xi}$ and the hypersingular kernel $l_1(\mathbf{x}-\boldsymbol{\xi})$ remains to be the main part of the integral operator, whereas, for a surface-breaking crack, the addition l_2 also becomes singular. Eq. (6.2), of course, is much more complicated than eq. (4.5). However, the explicit form of the kernels provides a chance to develop and implement low-cost numerical algorithms of its solution as well.

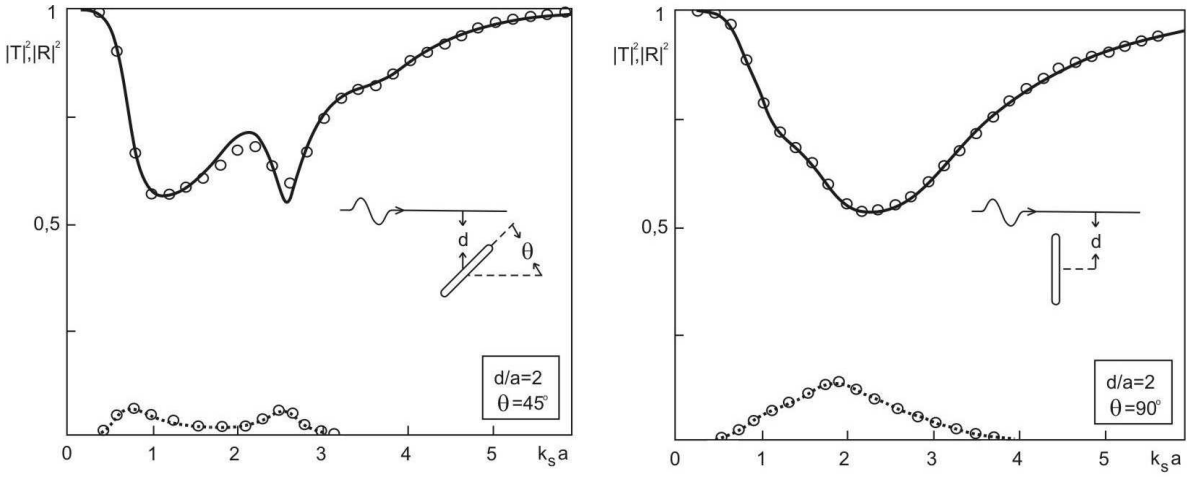

Figure 2: Transmission (solid line) and reflection (dot line) coefficients versus $\kappa_s a$ for inclined and vertical cracks accordingly to Ref. [19] and calculated using Eq. (6.2) (circle marks).

In a 2D statement such a code has been created and tested against the numerical results by Hijden and Neerhoff [19]. Figure 2 gives plots of the transmission and reflection coefficients $|T|^2$ and $|R|^2$ for a Rayleigh wave diffracted by a sub-surface crack of width $2a$, depth $z_c = -d$ and angle of inclination θ. There are plots versus $\kappa_s a$ for an elastic half-plane of Poisson's ratio $\nu = 1/3$ obtained in [19] also via BIEs but with another form of the kernel representation. The results computed using eq. (6.2) (1D BIEs with $\Omega \equiv [-a, a]$ in the case) are marked off by circles.

The agreement of the results verifies the correctness of the analytical calculations above. Together with the numerical control of the boundary condition $T_z(\mathbf{u}_1+\mathbf{u}_2)|_{z=0} = 0$ it proves indirectly the validity of the asymptotics (4.9), (5.7), as well as of the $\mathbf{u}_c = \mathbf{u}_1+\mathbf{u}_2$ plots given below.

7 Numerical examples

Since C-scan (pulse-echo) images computed for a probe moving across the surface were already presented (e.g. [15]), in this section we will concentrate on $\mathbf{u}_c$ surface patterns and A-scan pulses obtained at different surface points with a fixed probe position. These results are for deepened cracks when the first terms $\mathbf{u}_1^{(1)}$ and $\mathbf{u}_2^{(1)}$ provide a proper approximation of $\mathbf{u}_c$.

For definiteness sake, hereinafter all space sizes and distances are given in millimeters and frequencies in megahertz, although these units of length l_0 and of frequency f_0 may be changed simultaneously (e.g. to measure distances in wavelengths) just keeping the inverse proportion $l_0 = const/f_0$.

At first, let us consider surface imprints of the scattered field diffracted by a circular crack of radius 3 located under the co-ordinate origin ($x_c = y_c = 0$) at the depth $z_c = -60$. The incident field is radiated by a vertical 9 MHz P-probe: $\mathbf{q}_0 = \mathbf{e}_3$; (x_0, y_0) are the coordinates of the center of the contact area D, which is a 2×2 square in the case.

A set of plots in Figs. 3-4 is for several probe positions from a remote one at $(x_0, y_0) = (-60, 0)$ up to $(x_0, y_0) = (0, 0)$ above the crack with horizontal ($\theta = 0^o$, Fig. 3) and inclined ($\theta = 45^o$, Fig. 4) crack's orientation. They demonstrate how the patterns of the amplitude of displacements $|\mathbf{u}_c|$ at the surface $z = 0$ can look like depending on the probe location and crack's incline. The pictures are calculated in the plotted area 180×120 for a steel sample of P and S waves velocities $v_p = 5595$ m/s and $v_s = 3230$ m/s. The integral equation were solved using 97 nodes in the expansion (4.6). Since the matrix of the algebraic system, to which eq. (4.5) is reduced, can be inverted only one time, computation of the field everywhere except the first point involves only asymptotics (4.9) and (5.7) that is not too expensive. For example, these figures have been computed with a 700 MHz Pentium-III PC with an averaged speed of 150 points per second.

Since measurements by a piezoelectric probe are comparatively slow, the A-scan transient signals are usually obtained at a few receivers' positions with a fixed position of the source. The electrical output at the receiver is modeled by Auld's time-domain argument $\delta\Gamma(t)$. In view of the usual relation between the values in time and frequency domains:

$$\delta\Gamma(t) = \frac{1}{\pi}\mathrm{Re}\int\limits_{\omega_1}^{\omega_2} \delta\Gamma(\omega)e^{-i\omega t}d\omega$$

it can be calculated by numerical integration basing on the values $\delta\Gamma(\omega)$ computed for a dense enough set of frequencies covering the required band $[\omega_1, \omega_2]$.

Many numerical examples of A-scan pulses computed this way are presented in particular in the thesis [22]. For comparability sake, let us consider the same isotropic model, like in [22], with different positions of the same receiving probe in addition to the pulse-echo records given there (Fig. 5).

Figure 6 gives examples of $\delta\Gamma(t)$ for a vertical P-probe with the square contact domain 10×10, placed precisely above the horizontal square 6×6 crack, located at the depth $z_c = -30$ in an elastic half-space with $v_p = 5760$ m/s and $v_s = 3130$ m/s. The probe

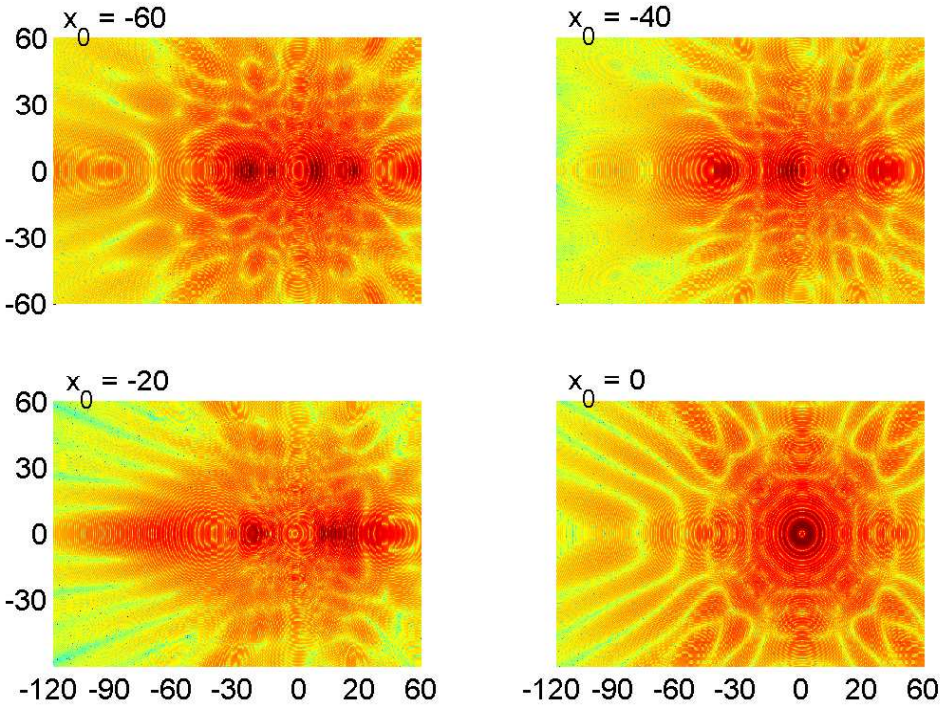

Figure 3: Reflected fields $|\mathbf{u}_c|$ with different probe positions; horizontal ($\theta = 0^o$) crack

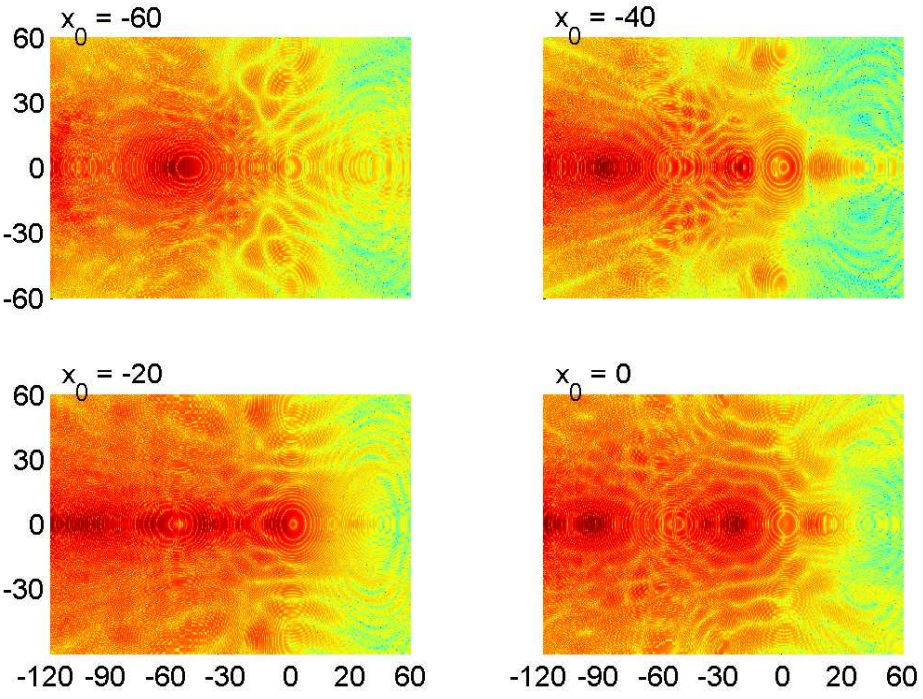

Figure 4: The same for a tilted ($\theta = -45^o$) crack

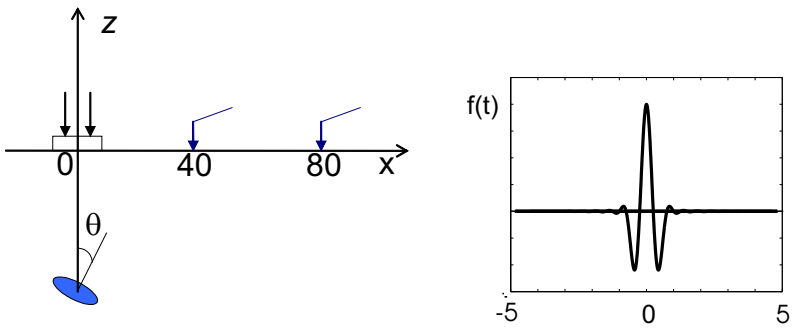

Figure 5: Allocation of receivers and the form of input signal

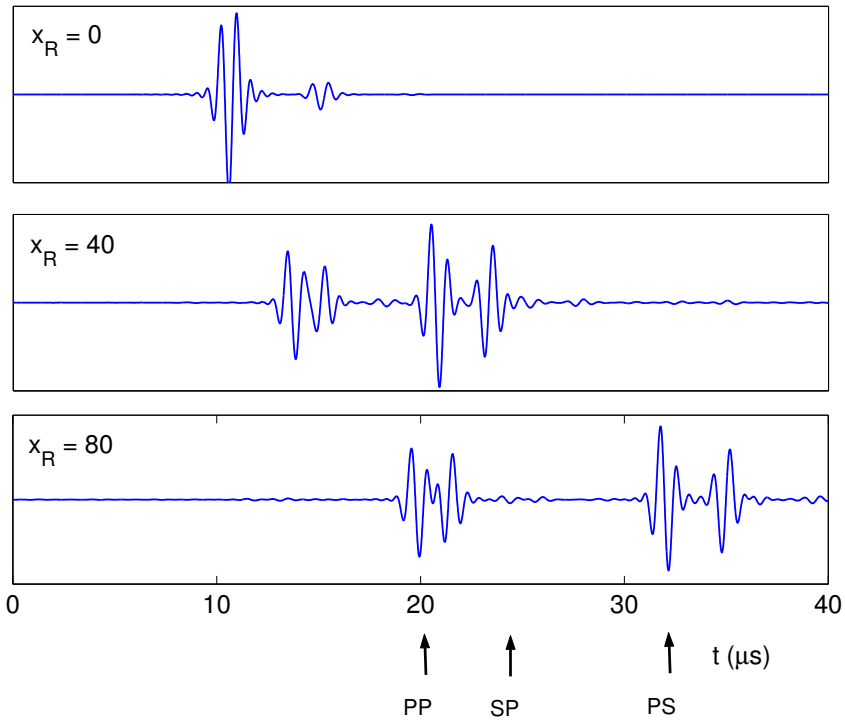

Figure 6: A-scan pulses $\delta\Gamma(t)$ at different receiving points for a horizontal square crack

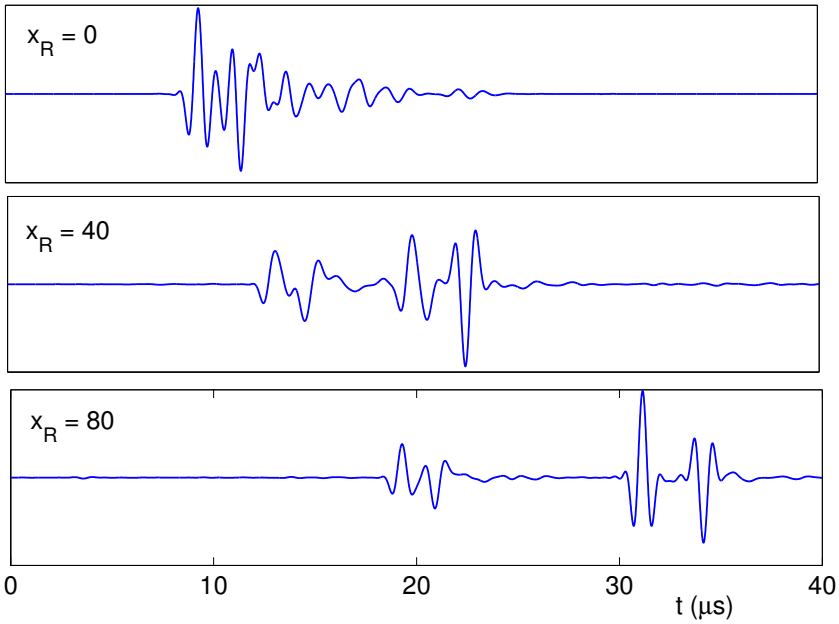

Figure 7: The same for an inclined ($\theta = 45^o$) elliptic crack

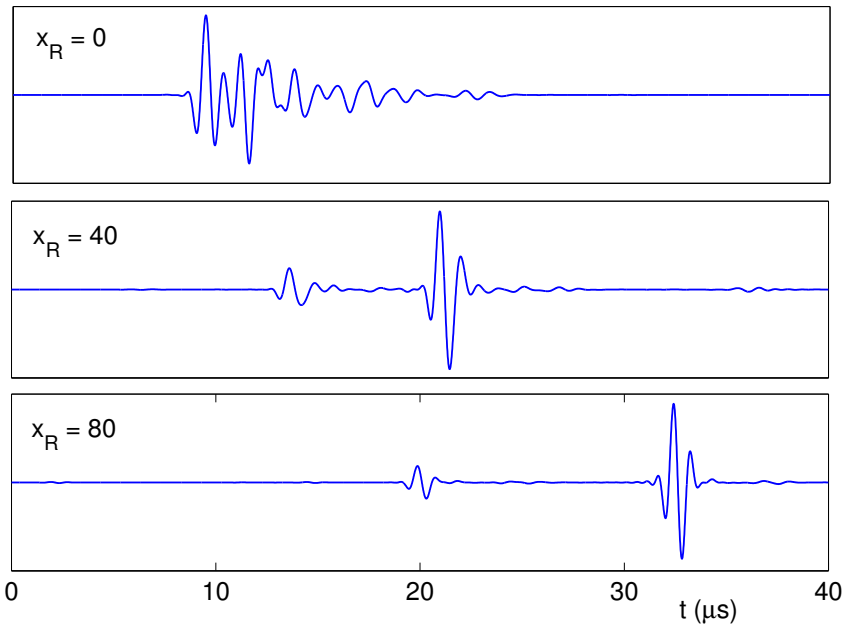

Figure 8: Calculated received signals $|\mathbf{u}_c(t)|$ for the same inclined ($\theta = 45^o$) elliptic crack

excites pulses with the frequency spectrum given in a limited band $|f - f_c| < \Delta f$:

$$F(\omega) = \cos^2\left(\frac{\pi(f - f_c)}{2\Delta f}\right), \quad \omega = 2\pi f$$

($F = 0$ if $|f - f_c| > \Delta f$). In the time-domain this spectrum yields a sharp signal. A draft of the signal associated with the central frequency $f_c = 1$ MHz and the bandwidth $\Delta f = 1$ MHz considered in the examples is shown in Fig. 5. In the Figs. 6-8 the time domain signals are normalized to fit the vertical size of subplots.

To calculate the plots $\delta\Gamma(t)$ one has, first, to compute values $\delta\Gamma(\omega_n)$ for a set of frequencies ω_n covering the required band with a certain frequency step h_f. In the examples below we used $h_f = 0.01$ MHz; that is eq. (4.5) had to be solved about two hundred times for different $\omega_n = 2\pi f_n$, $0 \le f_n \le 2$ MHz. Then those tabulated data were interpolated by splines so that the fast Fourier transform (FFT) procedure became applicable with any frequencies and time steps.

There are three positions of the center $\mathbf{x}_R = (x_R, 0, 0)$ of the receiving probe: $x_R = 0, 40$ and 80. The first is for the pulse-echo situation considered in [22]. Therefore, as expected, it looks very similar exhibiting the same arrival time of the reflected pulses. The maximal pulse at $t_{pp} = 10$ μs corresponds to the time of the PP response arriving; its duration is about 4 μs. Besides that, there is a small perturbation centered at the time of PS signal arriving $t_{ps} = 15$ μs and a very small SS signal at $t_{ss} = 20$ μs. The arrival of PP, PS, SP and SS wave packages becomes more visible at the remote point $x_R = 80$ with the total ray way $|\mathbf{x}_c| + |\mathbf{x}_R - \mathbf{x}_c| = 115.4$. The expected arrival times over this ray path $t_{pp} = 20, t_{sp} = 24.4$ and $t_{ps} = 32.5$ μs are indicated on the time axis by arrows.

Figure 7 displays $\delta\Gamma(t)$ at the same receiver positions but with the inclined elliptic crack (semiaxes $a = 4.8, b = 2.4$, $\theta = 45^o$), while Fig. 8 gives pulses $|\mathbf{u}_c(t)|$ for the same crack orientation. A correlation of these pictures shows that in spite of the variation of the signal's forms the records of $\delta\Gamma(t)$ and $|\mathbf{u}_c(t)|$ provide qualitatively similar information about the structure of scattered fields and about the times of different body waves arriving.

8 Summary

We have presented the analytically based low cost computer model of ultrasonic QNDE, which simulates wave processes excited and measured by both traditional piezoelectric transducers and novel laser devices.

The model looks like a useful tool for solution the inverse problem. It makes it possible to determine crack location by arrivals of scattered waves to different receiving points, as well as crack orientation and shape through the analysis of surface spots of maximal reflection and then by fine fitting of the surface patterns.

Along with NDT, the model developed can be used in geophysics.

9 Acknowledgements

We are thankful to Prof. A. Boström, Chalmers University of Technology, Sweden and to Prof. R. Kline, San Diego Center for Material Research, SDSU, USA for the support and fruitful discussions of NDT models. Various aspects of the model described were also discussed during a visit to the Centre for Automated and Robotic NDT, South Bank University, UK, supported by the Royal Society and London Mathematical Society. This work has also been supported by grants from the Russian Foundation for Basic Research (RFBR).

References

[1] J.D. Achenbach, A.K. Gautesen, H. McMaken, Ray methods for waves in elastic solids (with application to scattering by cracks). Pitman Advances Publishing Program (1982).

[2] V.M. Babich, V.S. Buldyrev, I.A. Molotkov, The Space-time Ray Method. Linear and Non-linear Waves, Leningrad, Leningrad University (1985) (in Russian).

[3] J.D. Achenbach, Wave Propagation in Elastic Solids, North-Holland, Amsterdam (1973).

[4] I.I. Vorovich, V.A. Babeshko, Dynamic Mixed Problems of Elasticity for Non-classical Domains, Nauka, Moscow (1974) (in Russian).

[5] V.A. Babeshko, E.V. Glushkov, and N.V. Glushkova, Energy vortices and backward fluxes in elastic waveguides, Wave Motion 16, 183-192 (1992).

[6] E.V. Glushkov, N.V. Glushkova, E.V. Kirillova, Normal mode diffraction in elastic layered waveguides; resonances and energy vortices, Proceedings of the Third International Conference on Mathematical and Numerical Aspects of Wave Propagation, Ed. G.Cohen, SIAM, Philadelphia, 604-612 (1995).

[7] E. Glushkov and N. Glushkova, Blocking property of energy vortices in elastic waveguides, J. Acoust. Soc. Am. 102(3), 1356-1360 (1997).

[8] W. Lin, L.M. Keer, Scattering by a planar three-dimensional crack, J. Acoust. Soc. Am., 82(4), 1442-1448 (1987).

[9] D.E. Budreck, J.D. Achenbach, Scattering from three-dimensional planar cracks by the boundary integral equation method, Journal of Applied Mechanics, 55, 405-412 (1988).

[10] A. Boström, Acoustic scattering by a sound-hard rectangle, J. Acoust. Soc. Am., 90(6), 3344-3347 (1991).

[11] L. Guan, A. Norris, Elastic wave scattering by rectangular cracks, Int.J.Solids Structures, 29(12), 1549-1565 (1992).

[12] C.J.S. Alves, T. Ha Duong, Numerical resolution of the boundary integral equations for elastic scattering by a plane crack, Int. J. Num. Mech. Eng., 38, 2347-2371 (1995).

[13] Ye.V. Glushkov and N.V. Glushkova, Diffraction of elastic waves by three-dimensional cracks of arbitrary shape in a plane, J. Appl. Maths Mechs 60(2), 277-283 (1996).

[14] L.M. Brekhovskikh, Waves in Layered Media, 2nd Ed., Academic Press, New York (1980).

[15] Ye.V. Glushkov, N.V. Glushkova, and A.V. Ekhlakov, Mathematical model of ultrasonic detection for three-dimensional interface cracks, J. Appl. Maths Mechs 66(1), 147-156 (2002).

[16] A. Boström and H. Wirdelius, Ultrasonic probe modeling and nondestructive crack detection, J. Acoust. Soc. Am. 97, 2836-2848 (1995).

[17] B.A. Auld, General electromechanical reciprocity relations applied to the calculation of elastic wave scattering coefficients, Wave Motion 1, 3-10 (1979).

[18] J.D. Achenbach, R.J. Brind, Scattering of surface waves by a sub-surface crack, Journal of Sound and Vibration 76(1), 43-56 (1981).

[19] J.H.M.T. van der Hijden, F.L. Neerhoff, Diffraction of elastic waves by a sub-surface crack (in-plane motion), J. Acoust. Soc. Am. 75(6), 1694-1704 (1984).

[20] I.Arias, J.D. Achenbach, A model for the ultrasonic detection of surface-breaking cracks by the scanning laser source technique, Wave Motion 39, 61-75 (2004).

[21] M. Abramowitz, and I.A. Stegun, (Editors) Handbook of Mathematical Functions, National Bureau of Standards (1970).

[22] T. Grahn, Scattering of elastic waves from inhomogeneities in solids, Application to Ultrasonic NDT, PhD thesis, Dept. of Appl. Mechs, Chalmers University of Technology, Göteborg, Sweden (2002).